JOURNAL OF MATERIALS SCIENCE 8 (1973) 1573–1580

Creep in pure and two phase nickel-doped alumina

A. CROSBY*, P. E. EVANS
Department of Metallurgy, University of Manchester, Institute of Science and Technology, Manchester, UK

Creep in pure and two phase nickel-doped alumina has been investigated in the stress range 0.70 to 4.57 kgf mm^{-2} (1000 to 6500 psi), and temperature range 1450 to 1800° C, for grain sizes from 15 to 45 μm (pure alumina) and 15 to 30 μm (nickel-doped alumina). The effect of stress, grain size and temperature on the creep rate suggests that diffusion controlled grain-boundary sliding is the predominant creep mechanism at low stresses and small grain sizes. However, the stress exponents show that some non-viscous boundary sliding occurs even at the lowest stresses investigated. This mechanism is confirmed by metallographic evidence, which shows considerable boundary corrugation in the deformed aluminas. At higher stresses and larger grain sizes the localized propagation of microcracks leads to high stress exponents in the creep rate equation. The nickel dopant, which introduces an evenly distributed spinel second phase into the alumina matrix, increases the creep rate and enhances boundary sliding and localized crack propagation. The weakening effect of the second phase increases with grain size, and tertiary creep occurs at strains of 0.5% and below in large grained material.

1. Introduction

Although the low temperature mechanical properties of nickel-doped alumina had been investigated in these laboratories [1], its behaviour at higher temperatures had not been established. The purpose of the present investigation, therefore, was to study the high temperature creep properties of nickel-doped aluminas and to compare the properties of these materials with pure aluminas prepared in a similar manner.

Much information has been reported concerning the creep properties of pure alumina (Heuer *et al* [2] have reviewed the literature in this field) but the relative importance of the main mechanisms cited (i.e. viscous diffusional creep, grain-boundary sliding, dislocation climb) is still unclear. However, it does appear that at low stresses diffusional creep is predominant, and Heuer *et al* have suggested that non-Newtonian grain-boundary sliding may be important at higher stresses.

2. Experimental procedure

2.1. Material

In the present investigation the starting material was alumina powder (total impurities less than 0.1%), which was ball milled and cold isostatically compacted at 47 kgf mm^{-2}. For the production of nickel-doped specimens, 2 wt % nickel powder was added to the alumina before ball milling, and the green compacts were sintered in air so that nickel oxide was formed which retarded grain growth. Sintering times of 30 min at 1700° C produce high density, fine grain size nickel-doped aluminas, but the grain sizes so formed would not be stable at the creep temperatures to be used. Sintering times of 15 to 20 h were, therefore, used to ensure equilibrium grain size in the specimens prepared for tests. Different grain sizes in each batch of material were produced by sintering at 1700, 1800 and 1900° C. The densities of the compacts, measured by a water displacement method, are summarized in Table I. Metallographic examination showed that the residual pores were trapped within the grains.

The grain sizes were determined from the relationship:

$$\bar{C} = \pi^2/16 \times \bar{D} \quad (1)$$

where $\bar{C}$ = average linear intercept (from

*Now at: Department of Metallurgy, University of Strathclyde, Glasgow, Scotland, UK.

TABLE I Sintering temperatures, densities and grain sizes of the alumina compacts

Alumina type and batch No.	Sintering temp. (°C)	Density (% Theoretical)	Average grain size (μm)
Pure (2)	1700	98.8	15
Pure (3)	1800	95.5	21
Pure (4)	1900	95.8	45
Nickel-doped (5)	1700	98.7	15
Nickel-doped (6)	1800	98.3	17
Nickel-doped (7)	1900	97.3	30

$\not<$ 500 grains/specimen), $\bar{D}$ = average grain diameter. Both aluminas sintered at 1700°C showed monomodal distributions of grain size, but the materials sintered at 1800 and 1900°C showed bimodal distributions. In the pure aluminas the secondary modes were only noticeable as levelling off or slight upward kinks in the distribution curves after the initial peak. The relative sizes of the frequency peaks were 15.0% at 4 μm, and 9.6% at 10 μm for the pure material sintered at 1800°C and 6.8% at 13.5 μm, and 4.1% at 29.5 μm for the pure material sintered at 1900°C. The more pronounced peaks in the nickel-doped materials gave values of 17.3% at 4 μm, and 14.3% at 8 μm for the 1800°C sintered material, and 10.2% at 5.5 μm, and 6.6% at 19.5 μm for the 1900°C sintered material. In each case a class intervals of 2 μm was used in the frequency calculations. By comparison the materials sintered at 1700°C gave modal frequencies of 22% at grain sizes of 3.5 μm (pure alumina), and 4 μm (nickel-doped alumina).

The occurrence of the pronounced bimodal distributions in the nickel-doped materials may be explained as follows. Electron probe microanalysis of the nickel-doped materials has revealed a two phase structure [3, 4], consisting of an alumina rich matrix containing dispersed nickel rich grains. The phase diagram determined by Lejus [5] for the system $NiO\text{-}Al_2O_3$ shows no solubility of NiO in nickel aluminate spinel at any temperature, and vanishingly small solubility of alumina in the spinel below 1300°C. However, non-stoichiometric spinels containing between 50 and 83 vol % alumina were found between 1300 and about 1900°C, i.e. an increase in solid solubility of alumina with rising temperature. Typical X-ray counts from nickel rich grains in our material indicate that non-stoichiometric spinels are retained during cooling to room temperature. The nickel content of the spinels varies between 11 and 33 wt %, and the larger spinel grains generally contain a higher proportion of nickel than the smaller grains. It also appears that the larger spinel grains grow at the expense of the smaller spinel grains, since they decrease in number but increase in size as the sintering temperature is raised. The sequence of events, therefore, appears to be complex involving oxidation of the nickel and solution of alumina to form non-stoichiometric spinels, and spinel grain growth by the transfer of nickel from smaller to larger spinel grains. Such inter-particle diffusion may lead to some segregation of nickel at the grain boundaries, as observed by Jorgensen and Westbrook [6]. If the rate of spinel grain growth depends on inter-particle nickel diffusion, the growth process will be strongly temperature dependent, and the rate of spinel grain growth may differ appreciably from alumina grain growth under the same temperature conditions. This would explain the clearly defined bimodal distributions in the nickel-doped materials sintered at 1800 and 1900°C.

2.2. Creep testing

Work by Poteat [7] suggests that the creep rate in compression is independent of the length to diameter ratio of the specimen in the range 1.5 to 2.5:1. The specimens were therefore ground to 0.1182 ± 0.0002 in. diameter and cut and faced to 0.2300 ± 0.0002 in. long. They were deformed in compression at stresses between 0.70 to 4.57 kgf mm^{-2} (1000 and 6500 psi) in the temperature range 1450 to 1800°C. The creep apparatus, described more fully elsewhere [4], basically consists of a carbon tube furnace with a loading head transmitting the load to the specimen via graphite pushrods. The specimen chamber was flushed with high purity argon. Specimen deformation was measured by a linear variable differential transformer in contact with the loading head, and the results were recorded on a potentiometric chart-recorder. The strain-rate range was 10^{-3} to 1% min^{-1} and, depending on strain-rate, strains of 0.5 to 6.0% were measured.

3. Results and discussion

The creep curves showed all three stages of creep – the duration of each stage depended on temperature, stress and grain size. The nickel-doped materials deformed more rapidly than the pure aluminas under the same creep conditions.

3.1. Temperature dependence of secondary creep rate

At least five specimens from each batch of material were deformed in creep using a constant stress of 2.11 kgf mm^{-2}. The temperature was varied from specimen to specimen of the same batch, but remained constant during each test. The results are summarized in Fig. 1 where the natural logarithm of the steady state strain-rate (% min^{-1}) is plotted against the reciprocal absolute temperature.

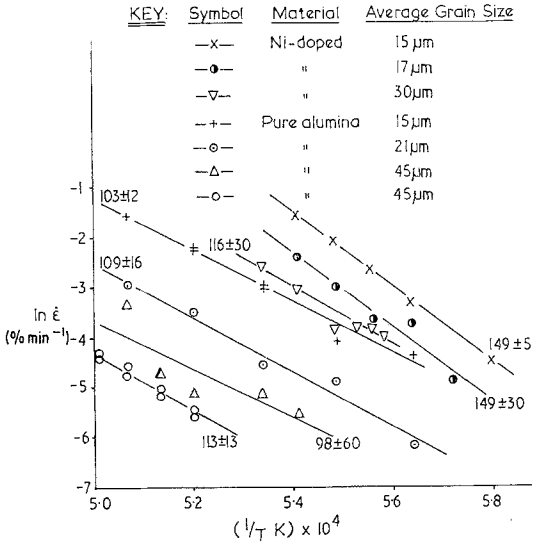

Figure 1 Temperature dependence of strain-rate for alumina at 2.11 kgf mm^{-2}. Figures quoted are activation energies for creep in kcal mol^{-1}.

The activation energies for creep derived from the best fit straight lines for pure alumina are consistent, within the limits of experimental accuracy, with the results of Paladino and Kingery [8] for aluminium ion diffusion. The larger scatter in the values for the largest grain size material could not have been caused by measurement errors, since a standardized experimental procedure was adopted for each creep test. Although one might expect larger measurement errors at lower strain-rates, these were effectively reduced by measurement over longer periods of time. The scatter is attributed to structural differences between individual specimens in this batch. This was confirmed by further tests using single specimens for activation energy determinations, when values of 112 $\pm$ 15k cal mol^{-1} were obtained.

The value of activation energy obtained for the largest grained nickel-doped material was not considered reliable because of the narrow range of strain-rates to which measurment was necessarily restricted (because of the low creep strain to fracture), and the high degree of scatter within this range. However, the activation energies obtained for the smaller grained nickel-doped aluminas were higher than those for the pure material. This may be owing to changes in solubility with temperature in the two phase ceramic, when endothermic heats of solution could affect the measured value of the creep activation energy. Another possibility is a change in Ni^{2+}:Ni^{3+} ion ratio with increasing temperature, when the creep activation energy would consist of a defect mobility term and a defect creation term. However, the emergence and gradual predominance of a second mechanism (where diffusional processes are not rate controlling) with increasing temperature could give rise to a high value of the activation energy for creep. Such a mechanism could be non-viscous grain-boundary sliding with localized crack propagation [9]. The exact contribution of each of these mechanisms to the higher observed activation energy for creep in the nickel-doped alumina is at present unknown, but grain-boundary sliding and localized crack propagation has been observed in the metallography of the creep-deformed specimens.

3.2. Stress dependence of the secondary creep rate

The dependence of creep rate on stress level was determined by creep testing at constant temperature, and adjusting the stress in the range 0.70 to 4.57 kgf mm^{-2}. At low stresses, the strain-rate at several stress levels could be determined in one creep test. At high stresses, however, the strain-rates were so rapid that only one stress level per specimen could be employed.

Fig. 2 shows the variation of strain-rate with stress. The data for the smallest grained pure alumina and the medium grained nickel-doped alumina could be divided into two stress regimes. This phenomenon has been observed by several other workers [9-12]. At the lowest stresses investigated the pure alumina showed a stress exponent typical of a slight departure from viscous flow. At higher stresses a considerable increase in the stress exponent shows the dominance of a non-viscous deformation process and the increased scatter shows the importance of

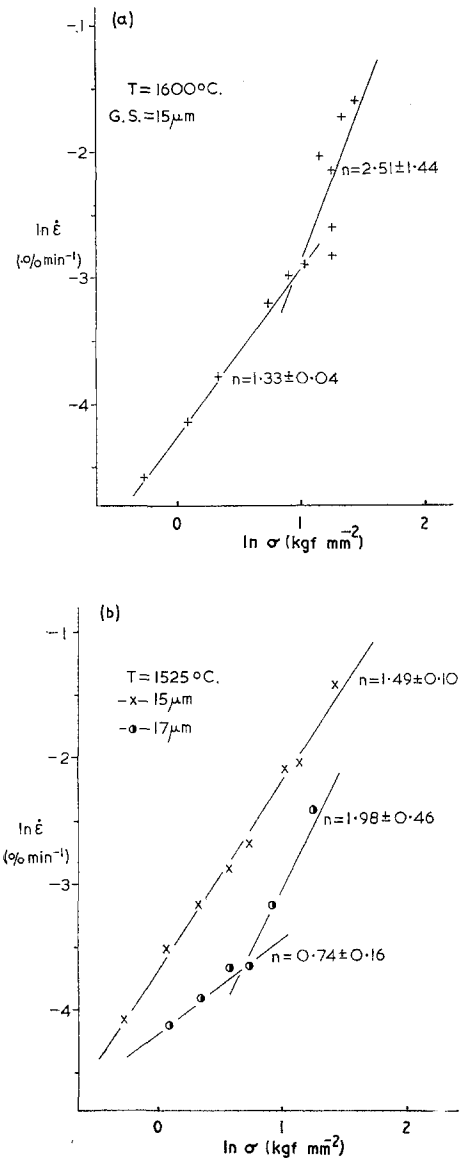

Figure 2 (a) Stress dependence of strain-rate for pure alumina. (b) stress dependence of strain rate for nickel-doped alumina.

individual specimen structure in determining the strain-rate in this regime. Metallographic evidence showed that non-viscous grain-boundary sliding and localized crack propagation was responsible for these high strain-rates. Coble and Guerard [13] attributed enhanced creep rates in alumina at large grain sizes and stresses to grain-boundary separation, and there, too, localized propagation of microcracks was probably responsible for the separations. The medium grain size nickel-doped alumina showed a stress-strain-rate relationship approximating to viscous behaviour at low stresses, but there was again a rapid increase in strain-rate at higher stress levels, giving a stress exponent showing the dominance of a non-viscous creep process.

The finest grained nickel-doped alumina did not show a sharp transition from low to high exponent regimes, but the stress exponent did show that non-viscous creep processes were occurring. It is possible that the interpretation of the data for the 15 μm material in Fig. 2b as a straight line is not justified, and that the stress exponent is changing with stress at the higher stresses, i.e. the transition may be beginning at the higher stresses in this range, leading to a value of stress exponent greater than unity when the two ranges are considered together.

3.3. Grain size dependence of strain-rate

For the creep tests performed at constant stress, the temperature-compensated strain-rate (z) was calculated from the creep rate equation in the following manner:

$$\dot{\epsilon} = k\,\sigma^n G^b\,\mathrm{e}^{-\Delta H/RT}$$

where k, n, b are constants, T = temperature in K, ΔH = activation energy for creep, $\dot{\epsilon}$ = strain rate, σ = stress, G = grain size

$$\therefore \ln \dot{\epsilon} = n\ln\sigma + b\ln G - \frac{\Delta H}{RT} + \text{constant}.$$

Since σ is constant in this series of tests,

$$\ln \dot{\epsilon} + \frac{\Delta H}{RT} = b\ln G + \text{constant} = z \qquad (2)$$

Because of the low creep strain to failure in the largest grained nickel-doped alumina,measurable strain-rates were only possible at low creep rates, and even so the degree of scatter and inaccuracies made these results unreliable. A reliable grain size dependence of creep rate was, therefore, not obtained for the nickel-doped material.

However, for the pure alumina the temperature-compensated strain-rate derived from Equation 2 using an average activation energy of 108 kcal mol^{-1}, was plotted against the logarithm of average grain size. The results are shown in Fig. 3. For the largest grained material three points are clearly well above the scatter limits one would normally expect, and this was attributed to differences in structure in these specimens. The regression line for the data gives

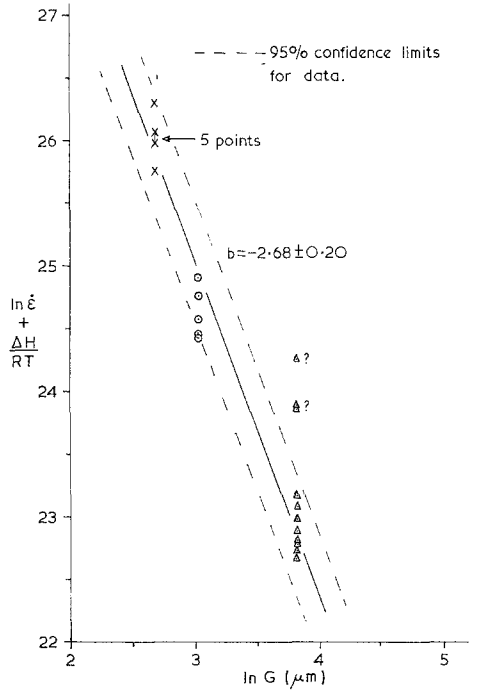

Figure 3 Grain size dependence of strain-rate for pure alumina at 2.11 kgf mm^{-2}.

a gradient of -2.68 ± 0.20. This lies between the grain size exponents expected for a mechanism controlled by diffusion through the grains (Nabarro-Herring [14], $b = -2$) and diffusion along the grain boundaries (Coble [15], $b = -3$), and suggests that more than one creep mechanism is involved in the deformation process. This result is similar to that of Heuer, *et al* [2] who found a grain size exponent of -2.5 for creep in alumina.

3.4. Microstructural changes during creep

After creep testing the specimens were sectioned along the stress axis and the polished surfaces were examined in reflected light. Etched specimens were examined by reflected light and by replication electron microscopy.

Fig. 4 shows the effect of increasing stress on the microstructure after creep. The specimen in Fig. 4a was deformed in the low stress exponent regime and shows grain-boundary porosity and the linking of pores to form a continuous crack in the maximum shear stress direction (in all the micrographs the applied stress axis is parallel to the shorter side of the micrograph). Fig. 4b shows more boundary porosity and linking of pores to form cracks, but several wedge-shaped

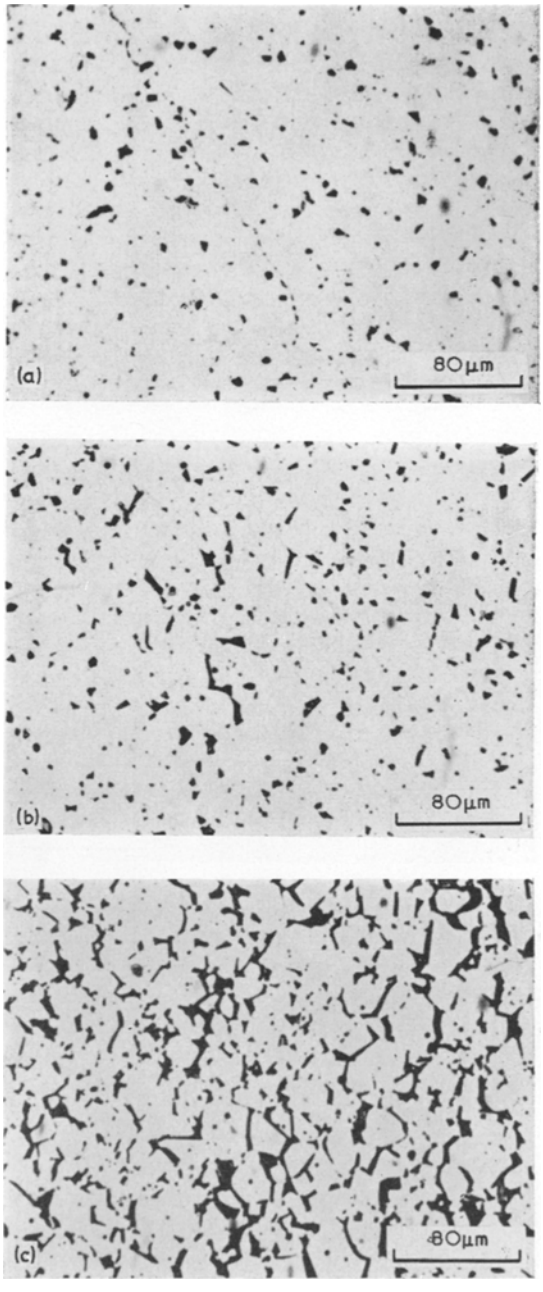

Figure 4 Pure alumina (batch 2) deformed at 1600°C, (a) 3.2% at 2.11 kgf mm^{-2}, (b) 5.4% at stresses from 2.46 to 3.52 kgf mm^{-2}. (c) 4.6% at 3.52 kgf mm^{-2} (unetched).

cracks are also visible. This microstructure is typical of a specimen deformed in the transition regime between low and high stress exponents. In the high stress exponent regime many wedge-shaped cracks, and straight-sided crack networks

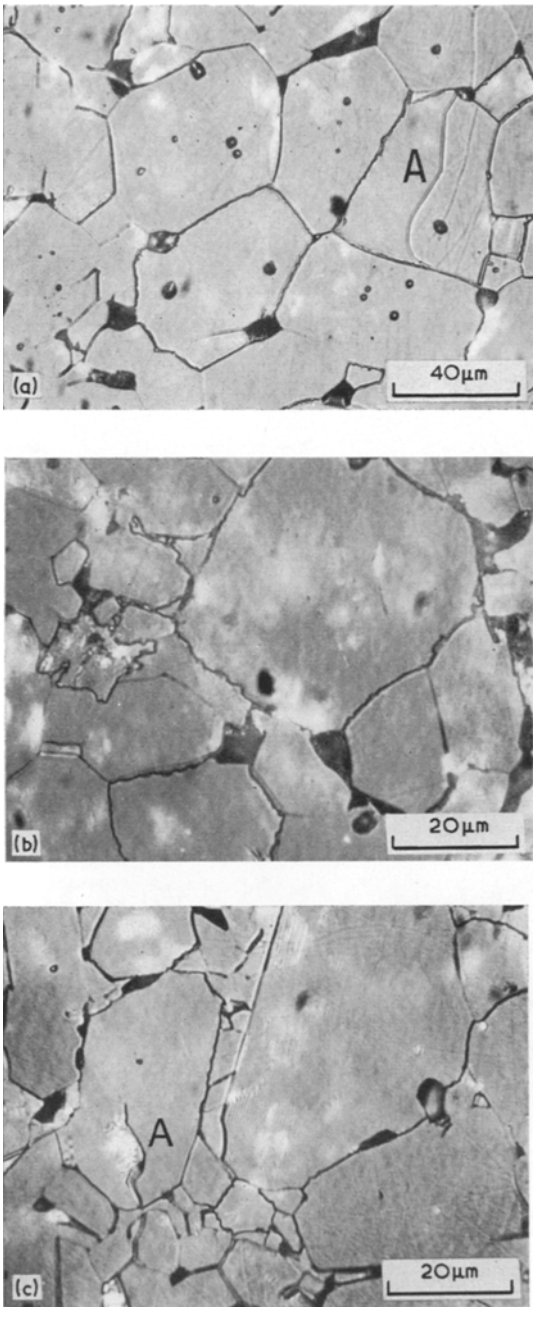

Figure 5 (a) Pure alumina (batch 4) deformed 1.1% at 1600°C and 2.11 kgf mm^{-2}. (b) Nickel-doped alumina (batch 6) deformed 2.7% at 1525°C and stresses from 1.05 to 1.76 kgf mm^{-2}. (c) Nickel-doped alumina (batch 5) deformed 5% at 1525°C and stresses from 0.70 to 1.76 kgf mm^{-2}. Etched in boiling phosphoric acid at 200°C.

were apparent, as shown in Fig. 4c. Both the pure and nickel-doped aluminas behaved in this fashion. Etching revealed considerable evidence of grain-boundary sliding in the form of grain-boundary corrugation, and cracking initiated at grain boundaries, as shown in Fig. 5. The light regions in Fig. 5 are caused by subsurface voids. In the nickel-doped aluminas whole grains shattered during the creep process, particularly in the largest grained material. A typical example is shown in Fig. 6 at A, and electron probe microanalysis of such areas has shown that the shattered grains are the nickel-rich phase.

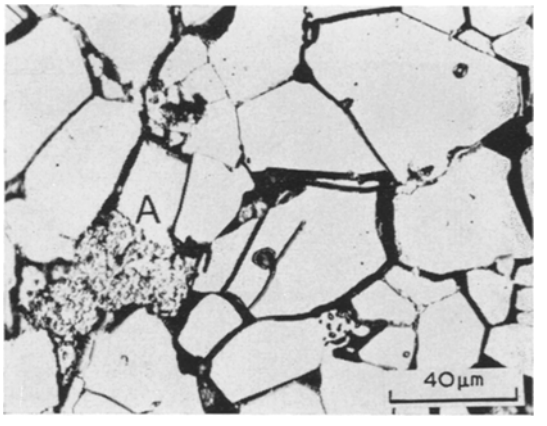

Figure 6 Nickel-doped alumina (batch 7) deformed 1.7% at 1575°C and 2.11 kgf mm^{-2}. Phosphoric acid etch.

Specimen failure occurred in a predominantly intercrystalline fashion, and the fracture path followed a plane at approximately 45° to the applied stress axis (Fig. 7).

4. Discussion

During grain-boundary sliding, stress concentrations are developed at obstacles in the sliding path (e.g. ledges, protrusions, pores, triple points), and further sliding may be inhibited by the back stresses so developed. Further sliding can only occur if these stresses are relieved in some way. This could occur by diffusional processes, dislocation mechanisms, or crack propagation. The limited number of slip systems available in alumina will restrict dislocation movement to those grains favourably oriented for slip to occur, and at low stresses diffusional processes should be the predominant stress relieving mechanism. The experimentally observed relationship between strain-rate, temperature and stress, supports the theory that a diffusional

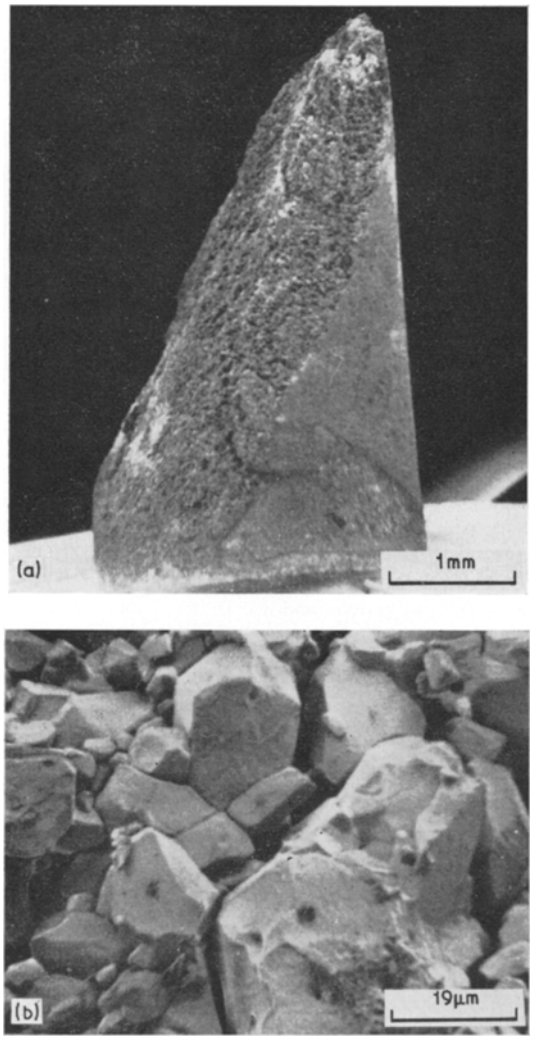

Figure 7 Pure alumina (batch 2) fractured at 2.0% strain at 1600° C and 4.22 kgf mm^{-2}. (a) Macroscopic direction of fracture path. (b) Intercrystalline fracture surface.

process is the dominant rate controlling step during creep at low stresses. However, at higher stresses the stress concentrations may be sufficiently high for initiation and local propagation of microcracks to occur. This would allow deformation to continue at a faster rate than a diffusion-controlled process, and would account for the increase in stress exponent at higher stresses. The metallographic evidence of an increasing number of wedge-like and straight-sided cracks with increasing stress exponent supports this hypothesis.

The larger grained materials also showed a higher proportion of wedge-like and straight-sided cracks than the smaller grained materials deformed under identical conditions of stress and temperature. Hence, the changeover in stress exponent must occur at lower stresses and/or temperatures in larger grained materials. The bigger grain facets in a larger grained material would allow pores to coalesce and form a crack of sufficient length for localized propagation to occur at stresses that would not induce propagation in a finer grained material with smaller facets. Transgranular cracks, which have been observed in our specimens (e.g. Fig. 5c) at A, will generally grow to a maximum length of one grain diameter and will be arrested at the grain boundary. The stress concentrations at the tips of these cracks will depend on their lengths, and further propagation will occur only in the longest cracks at a certain stress level. The larger grained materials will contain a higher proportion of long cracks than the finer grained materials, and propagation of these cracks will, therefore, play a more important role in larger grained materials. The effect of the nickel dopant was to increase the strain-rate and decrease the stress at which the transition in creep mechanisms occurred. The metallography shows a higher proportion of cracking in the nickel-doped materials. Indeed the extent of cracking in the largest grained nickel-doped aluminas was such that a tertiary creep stage was observed at strains of only 0.5% in some cases. The high strain-rates in the nickel-doped materials may be attributed to increased boundary sliding rates, and to an increase in the extent of localized crack propagation. An increase in the rate of sliding may be caused by enhanced boundary diffusion rates or by the formation of a viscous grain-boundary phase in the presence of nickel. Although such a nickel rich phase cannot be detected by electron probe microanalysis, Jorgensen and Westbrook [6] have shown by microhardness measurements, autoradiography, and lattice parameter measurements as a function of grain size, that nickel and magnesium oxides segregate to the grain boundaries in alumina doped with small quantities of these oxides.

5. Conclusions

1. At low stresses the stress, temperature and grain size dependencies of strain-rate for pure alumina show that the creep process is diffusion controlled and that the creep mechanism is slightly non-viscous in character (i.e. $\dot{\epsilon} \propto \sigma^n . G^b . e^{-\Delta H/RT}$, where $n = 1.33 \pm 0.04$,

$b = -2.68 \pm 0.20$, $\Delta H = 108 \pm 14$ kcal mol^{-1}. The non-integral stress and grain size exponents of creep rate suggest that several creep mechanisms are involved.

2. Grain-boundary corrugations are formed as a result of the sliding process, and transgranular microcracks are often initiated at sliding boundaries.

3. At higher stresses, stress exponents much greater than unity are observed, and metallographic evidence shows that the transition in creep mechanisms is associated with the localized propagation of microcracks.

4. The effect of nickel additions is to increase the strain-rate and increase the amount of crack propagation under given experimental conditions. The nickel additions are particularly detrimental to the creep properties of larger grained aluminas, since extensive cracking in the nickel-rich phase quickly leads to specimen failure.

5. The measured activation energy for creep in nickel-doped alumina was higher than in the pure material. This may be associated with the increase in localized crack propagation in this material, since the introduction of a non-diffusional mechanism for rapid creep would inevitably lead to erroneous activation energy values.

6. Tertiary creep and fracture occur by the growth and coalescence of the defects produced during secondary creep, and fracture is predominantly intercrystalline. The fracture path follows the direction of maximum shear stress.

References

1. (a). P. E. EVANS, B. P. HARDIMAN, B. C. MATHUR, and W. S. RIMMER, *Trans. Brit. Ceram. Soc.* **66** (1967) 523. (b). P. E. EVANS, *Brit. Pat. No. 1106327.*
2. A. H. HEUER, R. M. CANNON, and N. J. TIGHE, in: "Ultrafine Grain Ceramics" (eds. J. J. Burke, N. L. Reid, and Volker Weiss) Proceedings of the Fifteenth Sagamore Army Materials Research Conference (Syracuse University Press, 1970) pp. 339-365.
3. P. E. EVANS, in: "Materials Science Research" Vol. 3 (eds. W. W. Kriegel and H. Palmour III) (Plenum, New York, London, 1966) pp. 345-353.
4. A. CROSBY, Ph.D. Thesis, Manchester University (1971).
5. ANNE-MARIE LEJUS, Thesis, Faculté Des Sciences de l'université de Paris (1964).
6. P. J. JORGENSEN and J. H. WESTBROOK, *J. Amer. Ceram. Soc.* **47** (1964) 332.
7. L. E. POTEAT, Ph.D. Thesis, North Carolina State University, Raleigh, N.C. (1966); Univ. Microfilms (Ann Arbor, Mich.), Order No. 66-11, 978; 264 pp. *Dissertation Abstr. B*, **27** (1966) 1961.
8. A. E. PALADINO and W. D. KINGERY, *J. Chem. Phys.* **37** (1962) 957.
9. P. E. EVANS, *J. Amer. Ceram. Soc.* **53** (1970) 365.
10. J. H. HENSLER and G. V. CULLEN, *ibid* **51** (1968) 557.
11. J. A. C. MARPLES and A. HOUGH, U.K.A.E.A. Research Group Report AERE-R6421 (1970).
12. E. M. PASSMORE and T. VASILOS, *J. Amer. Ceram. Soc.* **49** (1966) 166.
13. R. L. COBLE and Y. H. GUERARD, *ibid* **46** (1963) 353.
14. C. HERRING, *J. Appl. Phys.* **21** (1950) 437.
15. R. L. COBLE, *ibid* **34** (1963) 1679.

Received 22 March and accepted 21 May 1973.